Electronic Supporting Information

Fe@Fe_3Ge_2 Nanoparticles for MR Imaging-Guided NIR-Driven Photodynamic Therapy *in Vivo*

Ping Zhou,[a] Lixing Pan,[a] Guang Deng,[a] Zhiguo Zhou,*,[a] Heng Zhao,[a] Chen Peng, *,[b] Shiping Yang*,[a]

[a] The Key Laboratory of Resource Chemistry of Ministry of Education, Shanghai Key Laboratory of Rare Earth Functional Materials, and Shanghai Municipal Education Committee Key Laboratory of Molecular Imaging Probes and Sensors, Shanghai Normal University, Shanghai 200234, China.

[b] Department of Radiology, Shanghai Tenth People's Hospital, Tongji University, Shanghai 200072, China.

Corresponding Author : zgzhou@shnu.edu.cn;cpengrr@tongji.edu.cn; shipingy@shnu.edu.cn.

Materials

$Fe(CO)_5$ was purchased from Development of Beijing Chemical Technology Co.; Ltd. Branch. oleylamine and 1-octadecene (ODE) were purchased from Acros. Oleic acid, hexamethyldisilazane, and germanium (IV) iodide were purchased from Alfa Aesar. Hexadecylamine (HDA) was purchased from Sigma-Aldrich. The cyclic peptide c(RGDyK) was purchased from Peptide International, Inc. DSPE-PEG_{2000} and DSPE-PEG_{2000}-NHS were purchased from Nanocs Inc. Singlet oxygen sensor green (SOSG) was purchased from Thermo Fisher Scientific. Caspase-3 (8G10) rabbit mAb, cytochrome c (D18C7) rabbit mAb, p53(1C12) mouse mAb, bax antibody, Bcl-2 (D17C4) rabbit mAb (mouse preferred) and GAPDH (D16H11) XP rabbit mAb were purchased from Univ-Bio (China). SOD and mannitol were purchased from Yuanye Bio-Technology Co.; Ltd (China).

Characterization

Characterization. TEM was performed using a JEOL JEM-2011 transmission electron microscope. XRD was measured on a Rigaku D/MAX 2250 diffractometer with Cu Kα radiation. Hydrodynamic diameter and Zeta potential were carried out on a Malvern Zetasizer Nano ZS model ZEN3600. The hysteresis loop was detected on a Quantum Design SQUID magnetometer. The laser of 660, 730, 808, and 980 nm were obtained from Shanghai Xilong Optoelectronics Technology Co.; Ltd. The concentration of Fe^{3+} ions was determined by inductively coupled plasma mass spectrometry (ICP-MS, Vistampxicp, Varian). UV-Vis-NIR absorption spectra were performed on a DU 730 UV-Vis-NIR spectrophotometer at room temperature. Flow cytometry (Beckman Coulter, USA) was used to carry out related experiments. All T_2-weighted MR images *in vivo* were acquired using a 3T MRI System (Siemens Magnetom Verio), and T_2-weighted MR images *in vitro* were acquired using a 3T MRI System (NM120-Analyst). Thermo Multiskan MK3 was used to carry out MTT assay experiments.

The evaluation of the generation of singlet oxygen ($^1O_2$) in an aquesous solution.

Singlet oxygen generation of PEG-MNPs was observed by the fluorescent probes ABDA. ABDA (20 μL, 1 mg mL^{-1}) in water was added in the mixture containing PEG-MNPs (3 mL, 100 μg mL^{-1}). A solution of PEG-MNPs saturated with NaN_3 and ABDA, and a solution with ABDA only were used as control experiments. Each group was irradiated with 808 nm (1.27 W cm^{-2}) for 1 min and was cycled 30 times. After the illumination of the laser with the wavelength of 660, 730, 808, and 980 nm for every minute, respectively, the fluorescence spectra of ABDA were recorded every one minute.

MRI in solution.

The different concentrations of PEG-MNPs were tested on a 0.5 T system for T_2-weighted MRI by using a conventional spin-echo sequence. The MRI parameters were shown as follows: TR = 6000 ms, TE = 200 ms, RG1 = 25 db, DRG1 = 3, SW = 100 kHz. The concentration of Fe^{3+} in solution was tested by ICP-AES.

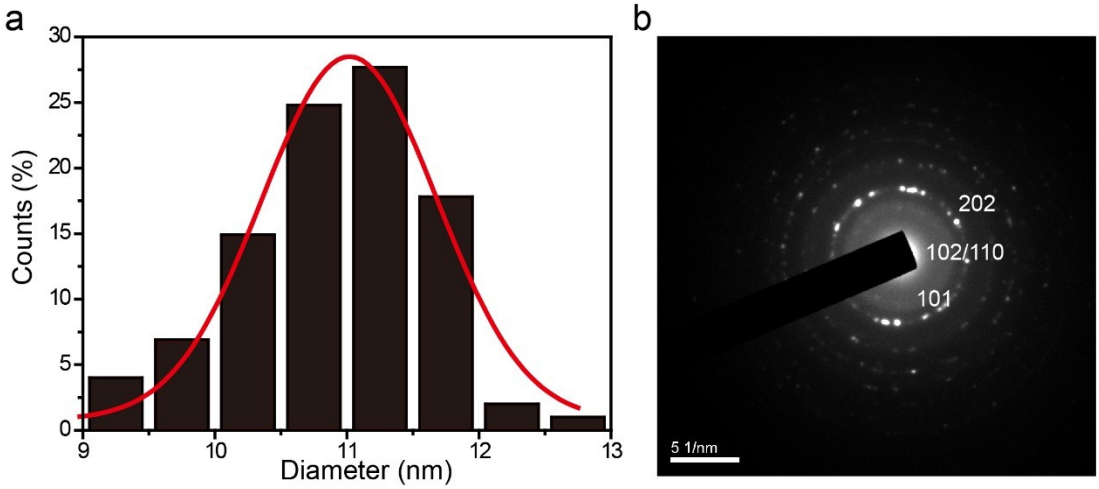

Figure S1. (a) TEM size distribution of MNPs. (b) The SAED pattern of $Fe@Fe_3Ge_2$ NPs.

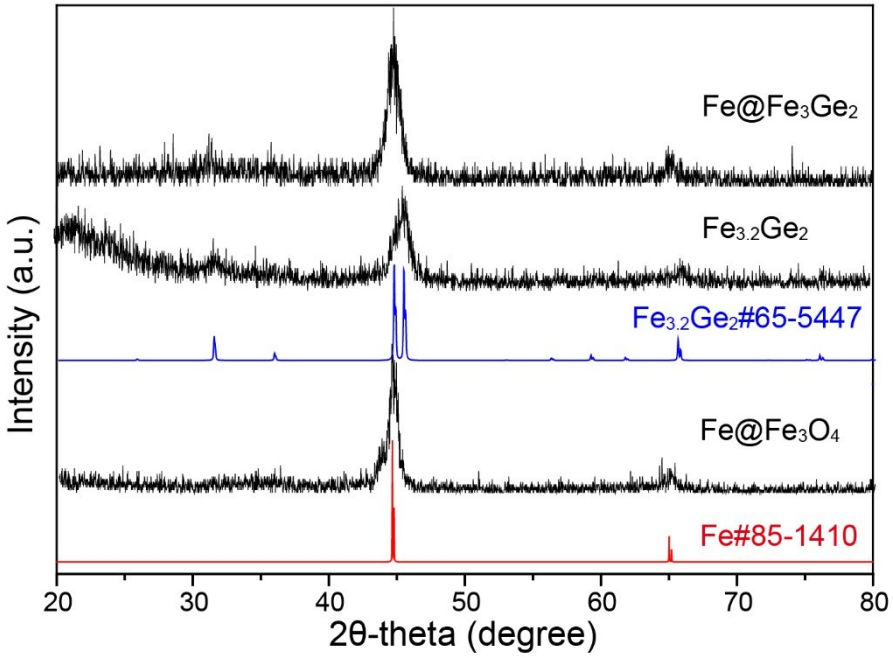

Figure S2. The XRD of $Fe@Fe_3Ge_2$, Fe_3Ge_2 and $Fe@Fe_3O_4$.

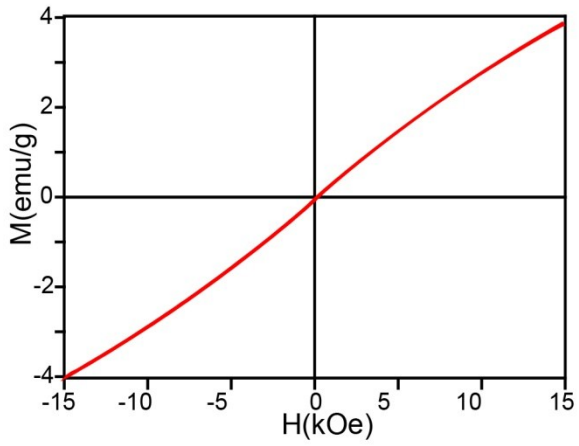

Figure S3. The hysteresis loop of Fe_3Ge_2 NPs.

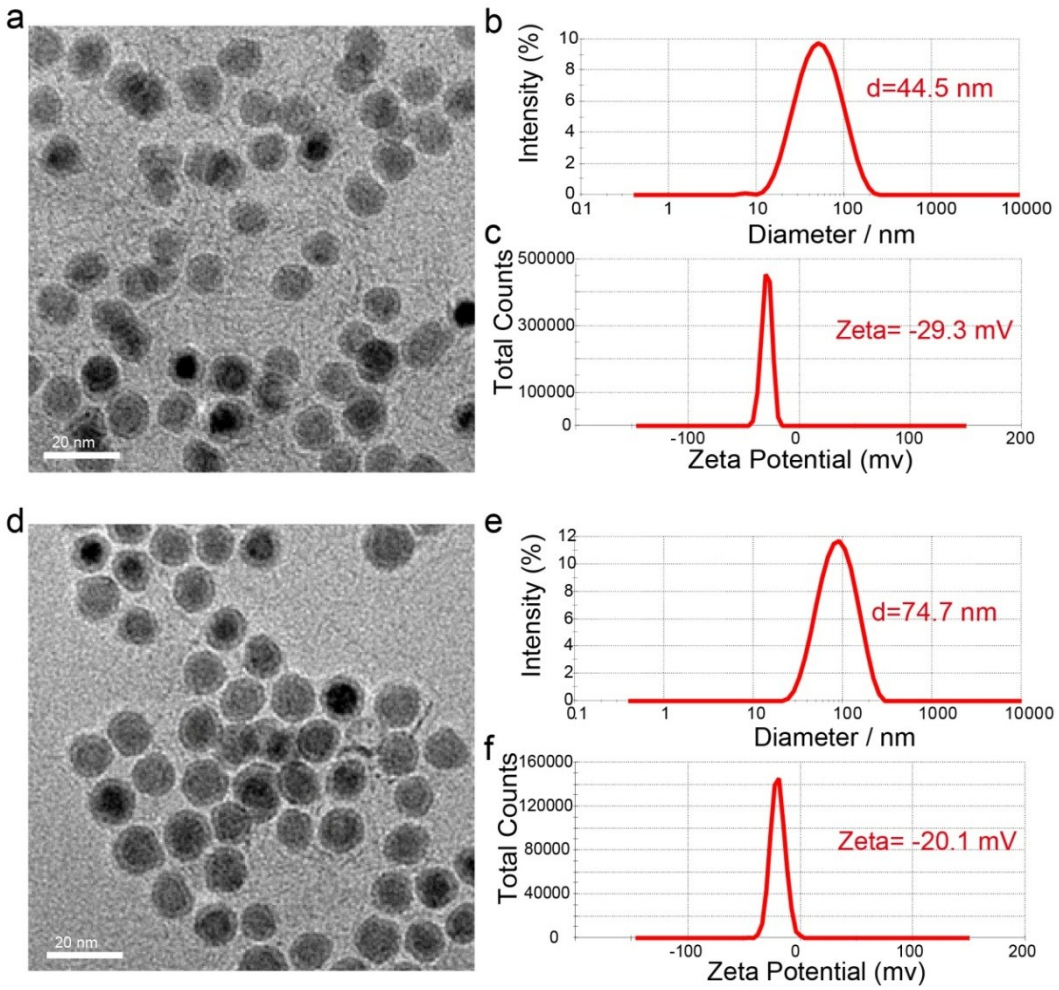

Figure S4. The TEM image (a), hydrodynamic diameter (b), and Zeta potentials (c) of PEG-MNPs, respectively. The TEM image (d), hydrodynamic diameter (e), and Zeta potentials (f) of RGD-MNPs, respectively.

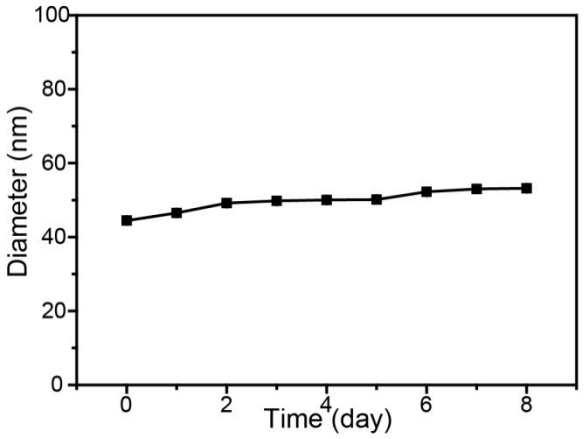

Figure S5. The change of the hydrodynamic diameter of PEG-MNPs in DMEM with 10% FBS as a function of time at 37 ^{o}C. Error bars were based on standard deviations of triplicated measurements.

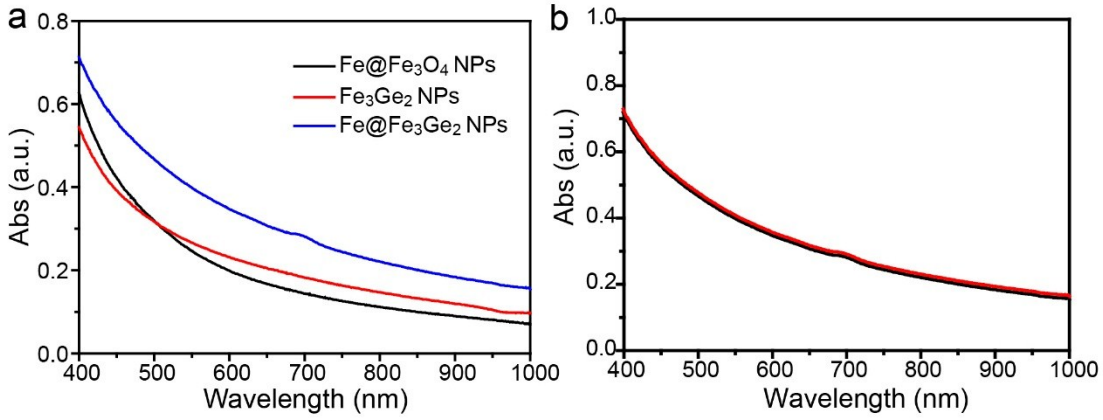

Figure S6. (a) The absorption spectra of $Fe@Fe_3O_4$ NPs (100 μg mL^{-1}), Fe_3Ge_2 NPs (100 μg mL^{-1}), PEG-MNPs (100 μg mL^{-1}). (b) The absorption spectra of PEG-MNPs (100 μg mL^{-1}) before (black) and after (red) the 808 nm laser irradiation (1.27 W cm^{-2}, 30 min).

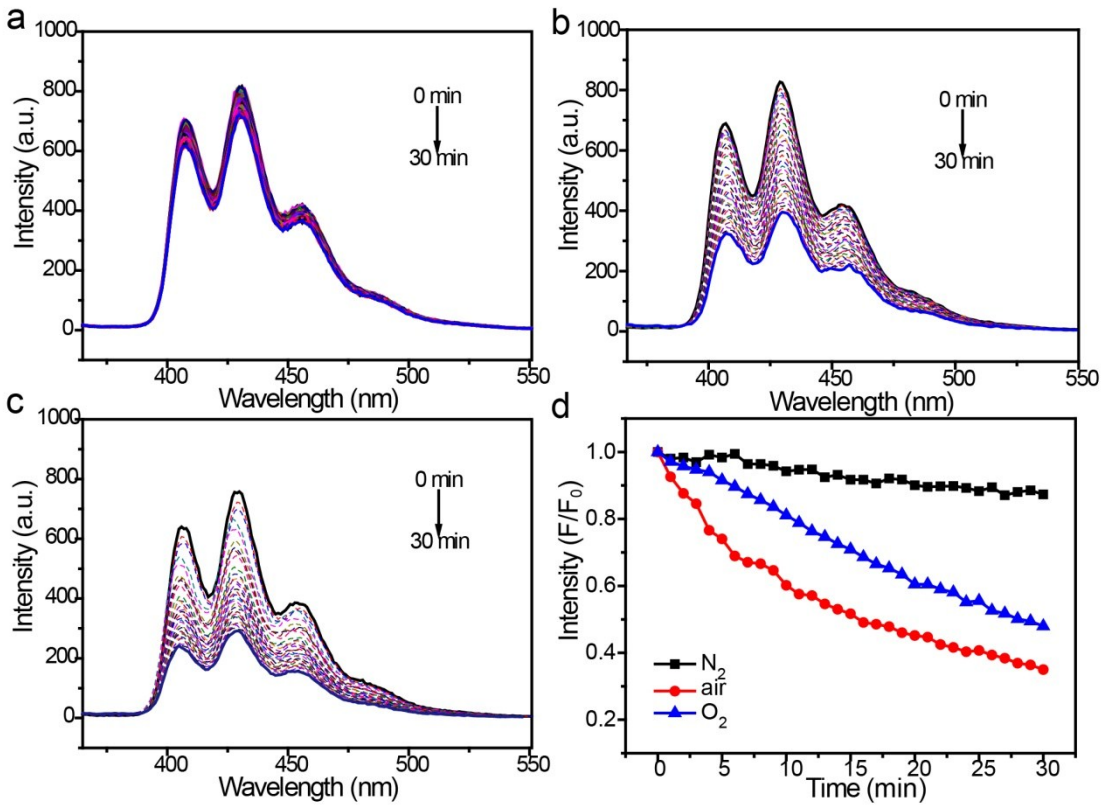

Figure S7. The changes of the fluorescence intensity of ABDA (6.7 μg mL^{-1}) in the presence of PEG-MNPs (100 μg mL^{-1}) irradiated by an 808 nm laser (1.27 W cm^{-2}) for 30 min under the N_2 (a), air (b) and O_2 (c) conditions. (d) The decay profiles of the fluorescence of ABDA centred at 430 nm in the presence of PEG-MNPs under the different conditions.

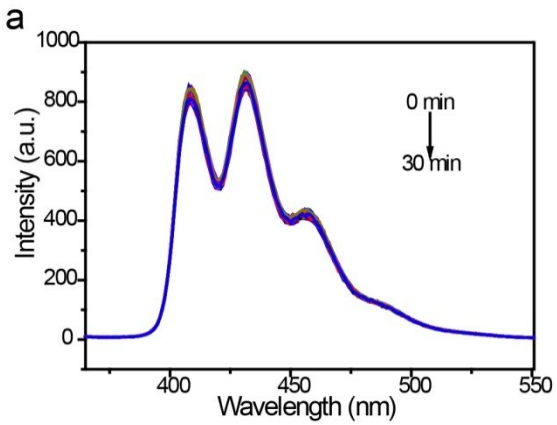

Figure S8. The production of singlet oxygen by PEG-MNPs in the presence of NaN_3 (420 μg mL^{-1}) under 808 nm laser irradiation, respectively.

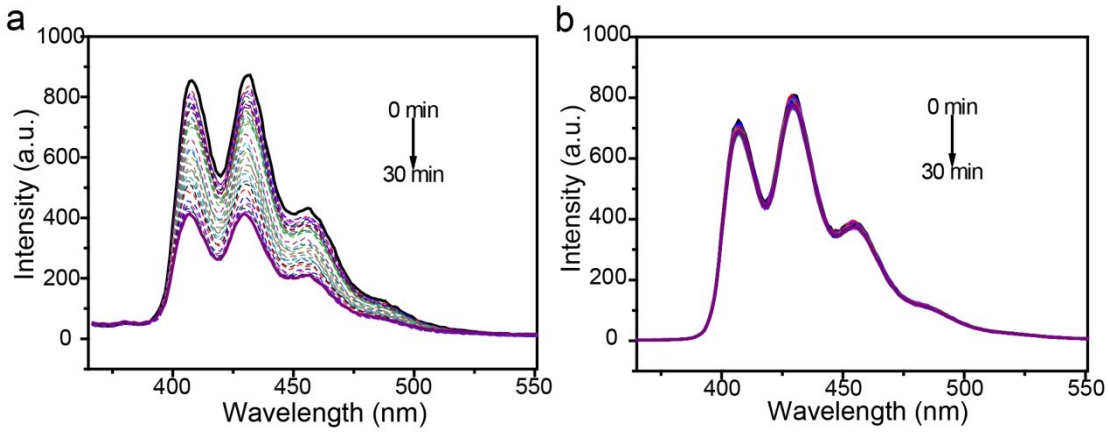

Figure S9. The changes of the fluorescence intensity of ABDA (6.7 μg mL^{-1}) in the presence of Fe_3Ge_2 NPs (a) and $Fe@Fe_3O_4$ NPs (b) under the 808 nm laser irradiation (1.27 W cm^{-2}) for 30 min, respectively. The concentration was 100 μg mL^{-1}.

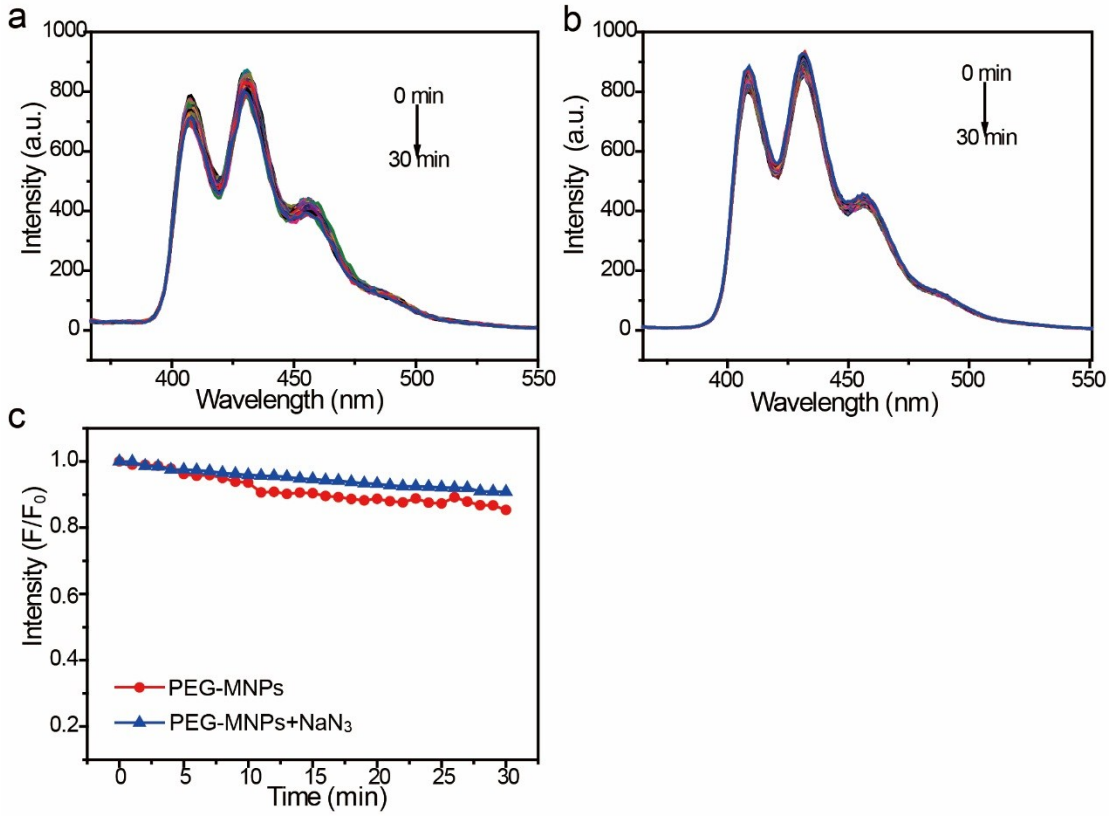

Figure S10. The changes of the fluorescence intensity of ABDA (6.7 μg mL^{-1}) in the presence of PEG-MNPs (100 μg mL^{-1}) without (a) and with (b) NaN_3 (420 μg mL^{-1}) under the 660 nm CW laser irradiation (1.27 W cm^{-2}) for 30 min, respectively. (c) The corresponding decay profiles of the fluorescence of ABDA centred at 430 nm in the presence of PEG-MNPs and PEG-MNPs + NaN_3 under the 660 nm laser irradiation, respectively.

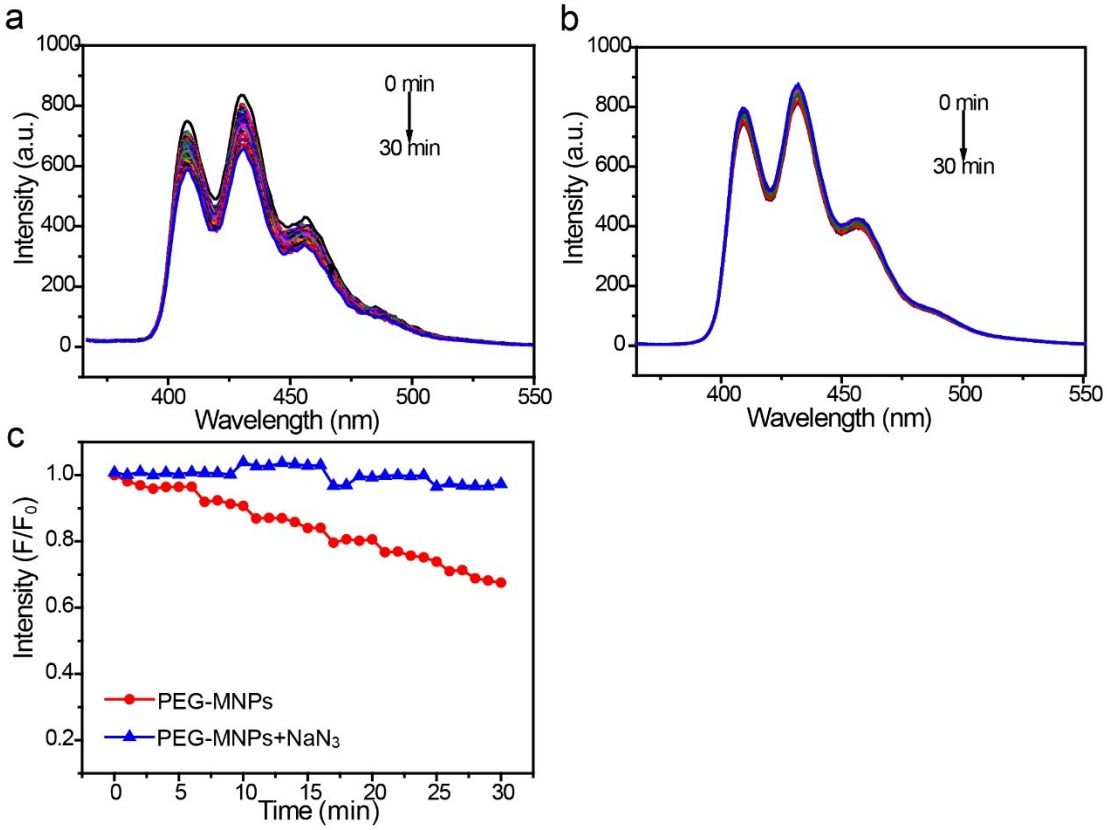

Figure S11. The change of the fluorescence intensity of ABDA (6.7 μg mL^{-1}) in the presence of PEG-MNPs (100 μg mL^{-1}) without (a) and with (b) NaN_3 (420 μg mL^{-1}) under the 730 nm CW laser irradiation (1.27 W cm^{-2}) for 30 min. (c) The corresponding decay profiles of the fluorescence of ABDA centred at 430 nm in the presence of PEG-MNPs and PEG-MNPs + NaN_3 under the 730 nm laser irradiation, respectively.

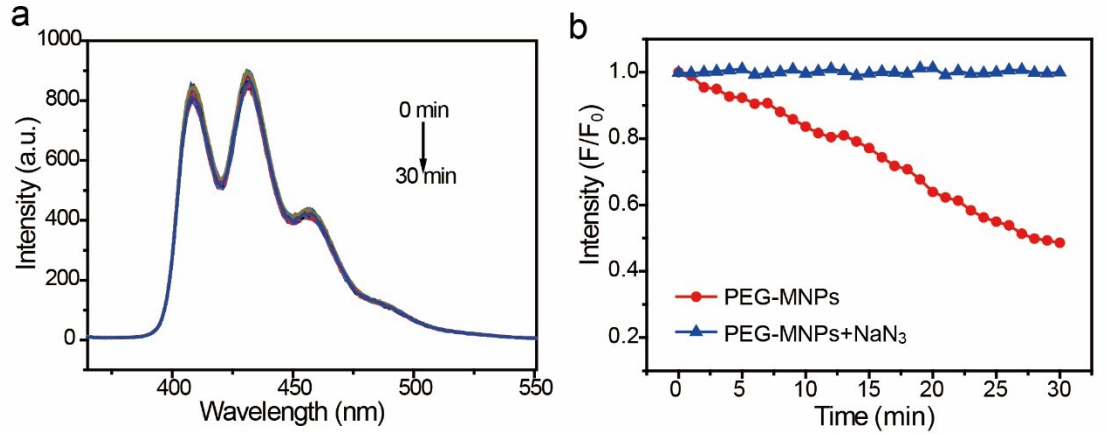

Figure S12. (a) The change of the fluorescence intensity of ABDA (6.7 μg mL^{-1}) in the presence of PEG-MNPs (100 μg mL^{-1}) without NaN_3 (420 μg mL^{-1}) under the 808 nm CW laser irradiation (1.27 W cm^{-2}) for 30 min. (b) The corresponding decay profiles of the fluorescence of ABDA centred at 430 nm in the presence of PEG-MNPs and PEG-MNPs + NaN_3 under the 808 nm CW laser irradiation, respectively.

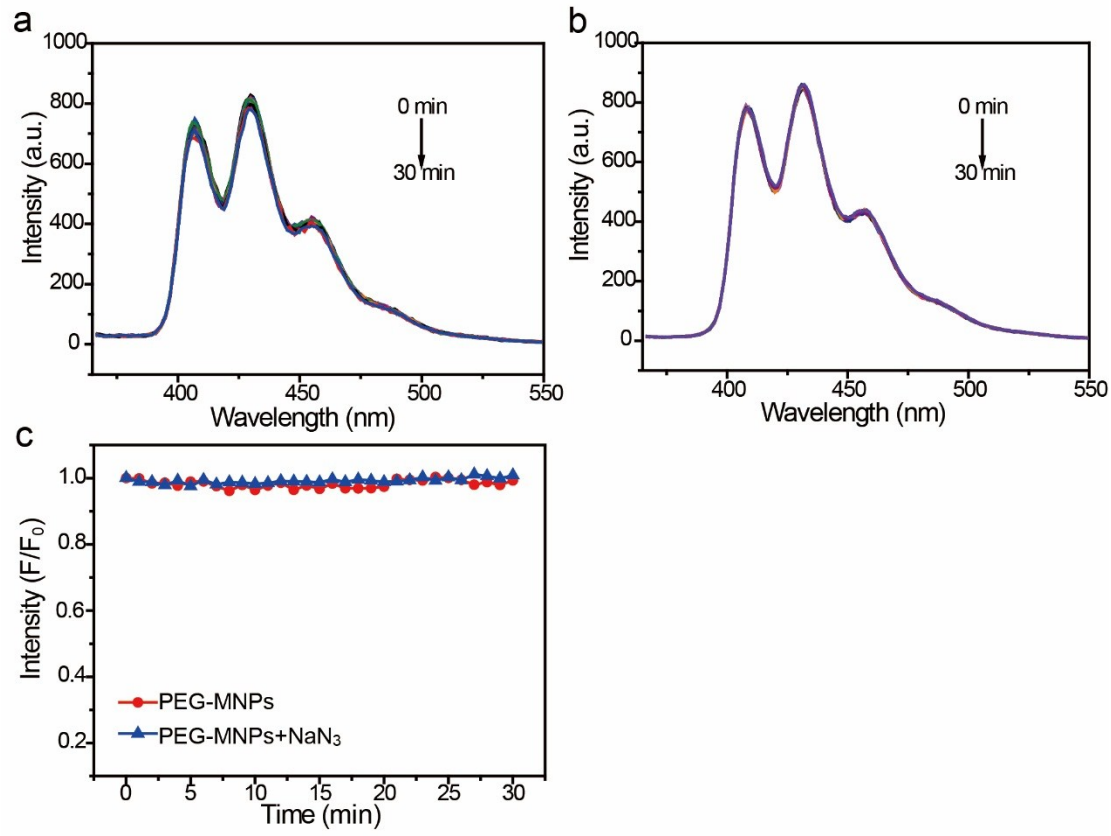

Figure S13. The change of the fluorescence intensity of ABDA (6.7 μg mL^{-1}) in the presence of PEG-MNPs (100 μg mL^{-1}) without (a) and with (b) NaN_3 (420 μg mL^{-1}) under the 980 nm CW laser irradiation (1.27 W cm^{-2}) for 30 min. (c) The corresponding decay profiles of the fluorescence of ABDA centred at 430 nm in the presence of PEG-MNPs and PEG-MNPs + NaN_3 under the 980 nm CW laser irradiation.

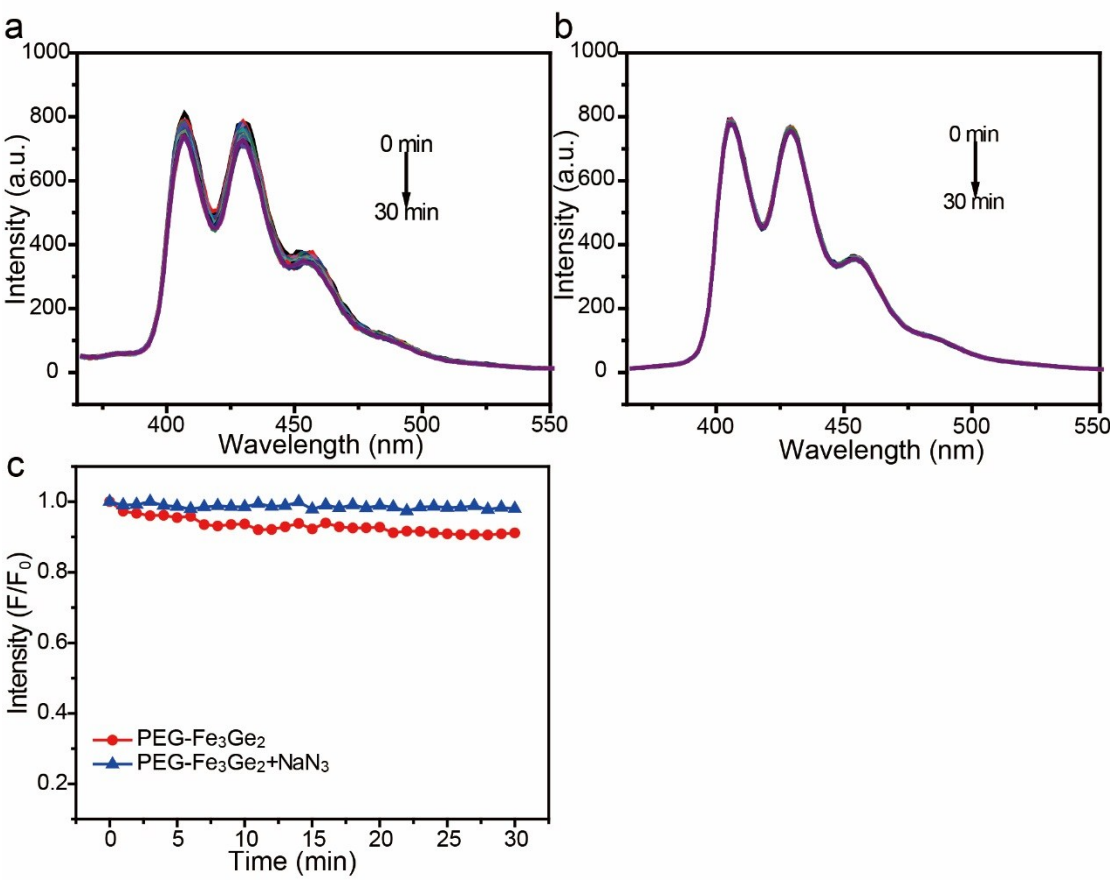

Figure S14. The changes of the fluorescence intensity of ABDA (6.7 μg mL^{-1}) in the presence of PEG-Fe_3Ge_2 (100 μg mL^{-1}) without (a) and with (b) NaN_3 (420 μg mL^{-1}) under the 660 nm CW laser irradiation (1.27 W cm^{-2}) for 30 min, respectively. (c) The corresponding decay profiles of the fluorescence of ABDA centred at 430 nm in the presence of PEG-Fe_3Ge_2 and PEG-Fe_3Ge_2 + NaN_3 under the 660 nm laser irradiation, respectively.

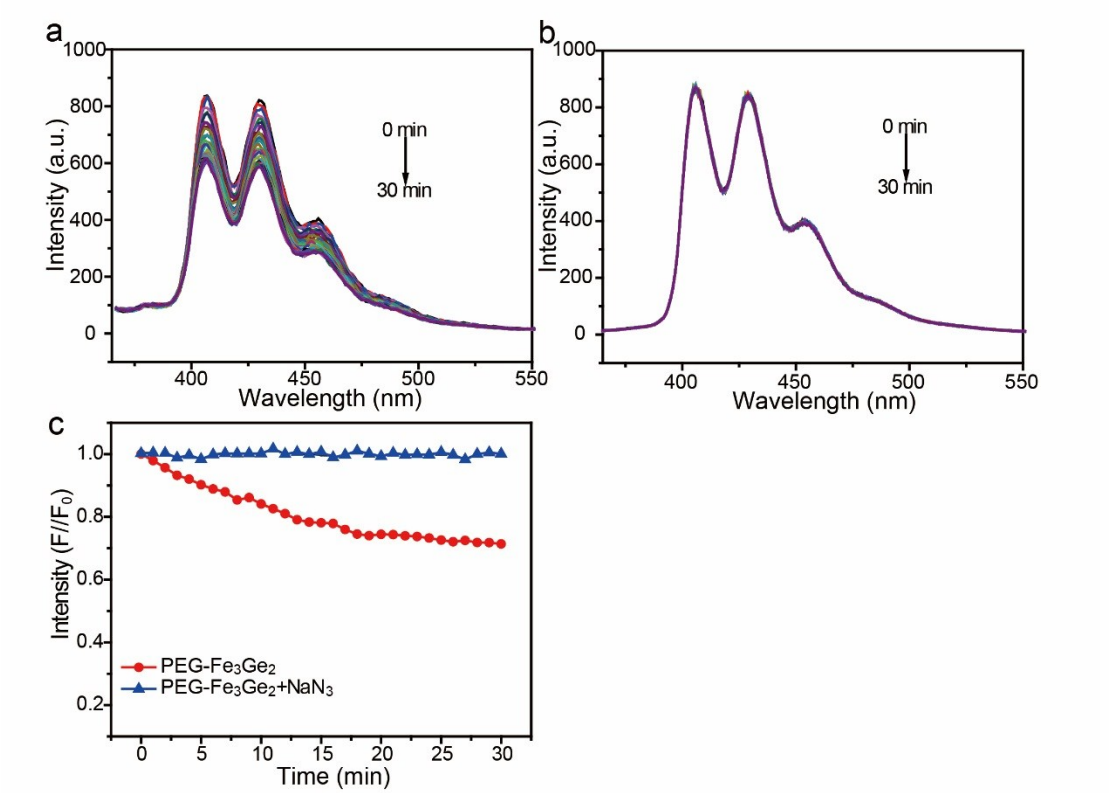

Figure S15. The changes of the fluorescence intensity of ABDA (6.7 μg mL^{-1}) in the presence of PEG-Fe_3Ge_2 (100 μg mL^{-1}) without (a) and with (b) NaN_3 (420 μg mL^{-1}) under the 730 nm CW laser irradiation (1.27 W cm^{-2}) for 30 min, respectively. (c) The corresponding decay profiles of the fluorescence of ABDA centred at 430 nm in the presence of PEG-Fe_3Ge_2 and PEG-Fe_3Ge_2 + NaN_3 under the 730 nm laser irradiation, respectively.

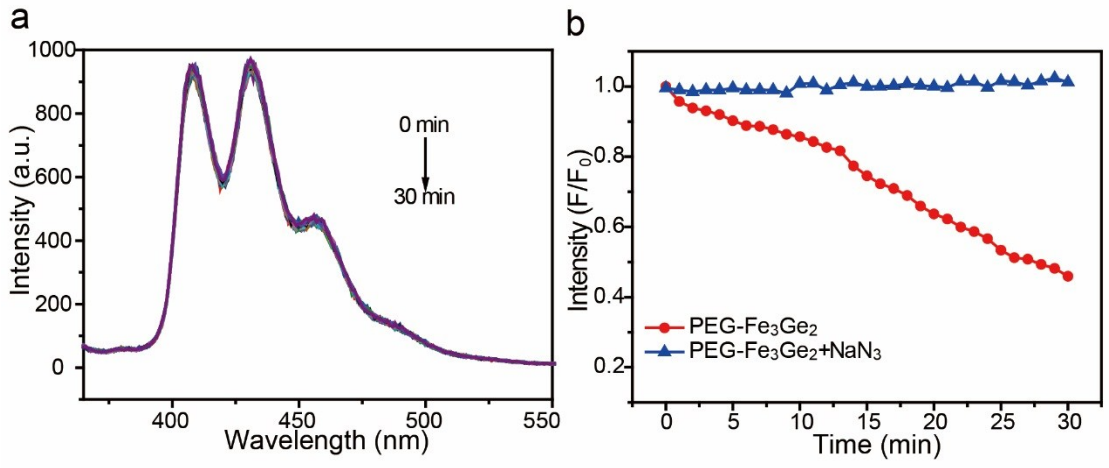

Figure S16. (a) The changes of the fluorescence intensity of ABDA (6.7 μg mL^{-1}) in the presence of PEG-Fe_3Ge_2 (100 μg mL^{-1}) with NaN_3 (420 μg mL^{-1}) under the 808 nm CW laser irradiation (1.27 W cm^{-2}) for 30 min. (b) The corresponding decay profiles of the fluorescence of ABDA centred at 430 nm in the presence of PEG-Fe_3Ge_2 and PEG-Fe_3Ge_2 + NaN_3 under the 808 nm laser irradiation, respectively.

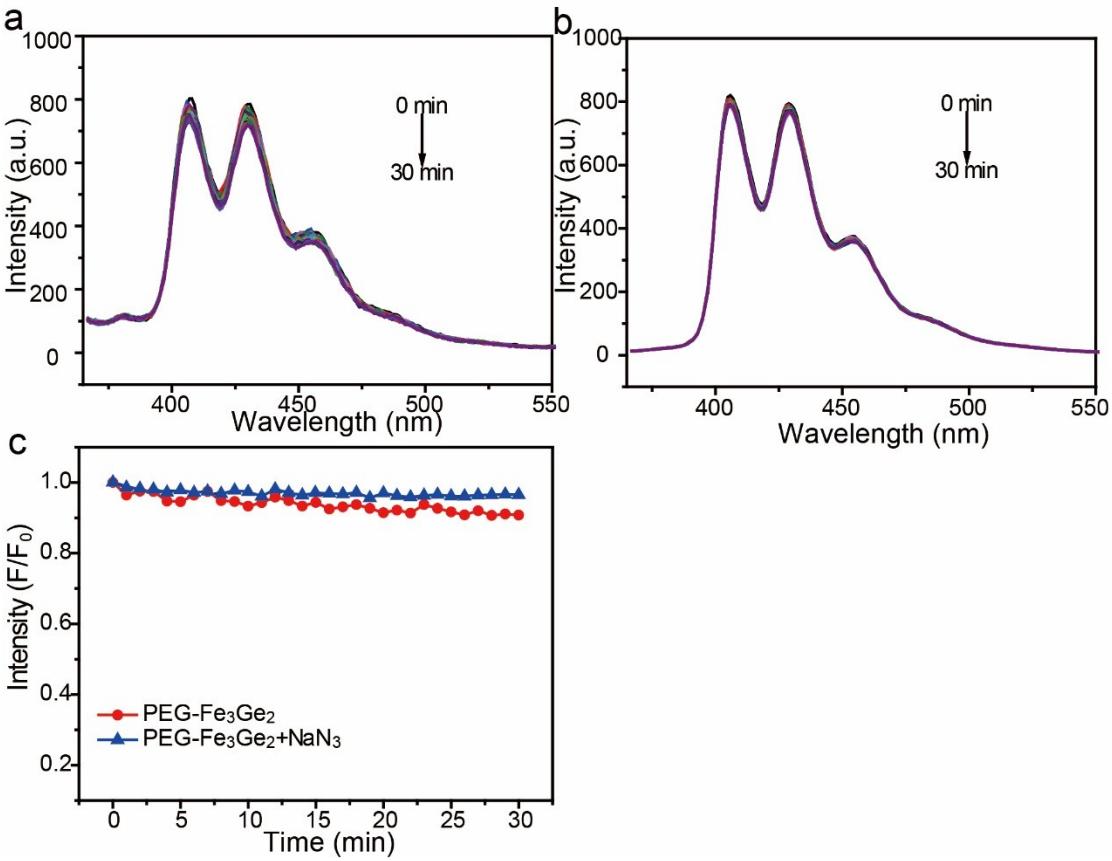

Figure S17. The changes of the fluorescence intensity of ABDA (6.7 μg mL^{-1}) in the presence of PEG-Fe_3Ge_2 (100 μg mL^{-1}) without (a) and with (b) NaN_3 (420 μg mL^{-1}) under the 980 nm CW laser irradiation (1.27 W cm^{-2}) for 30 min, respectively. (c) The corresponding decay profiles of the fluorescence of ABDA centred at 430 nm in the presence of PEG-Fe_3Ge_2 and PEG-Fe_3Ge_2 + NaN_3 under the 980 nm laser irradiation, respectively.

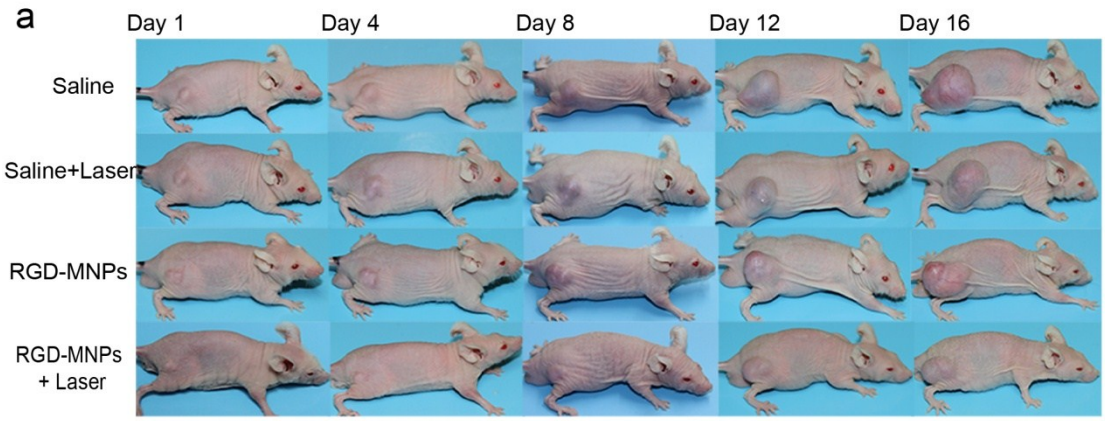

Figure S18. (a) Photographs of mice of different groups of mice after various treatments for 1, 4, 8,12 and 16 days.

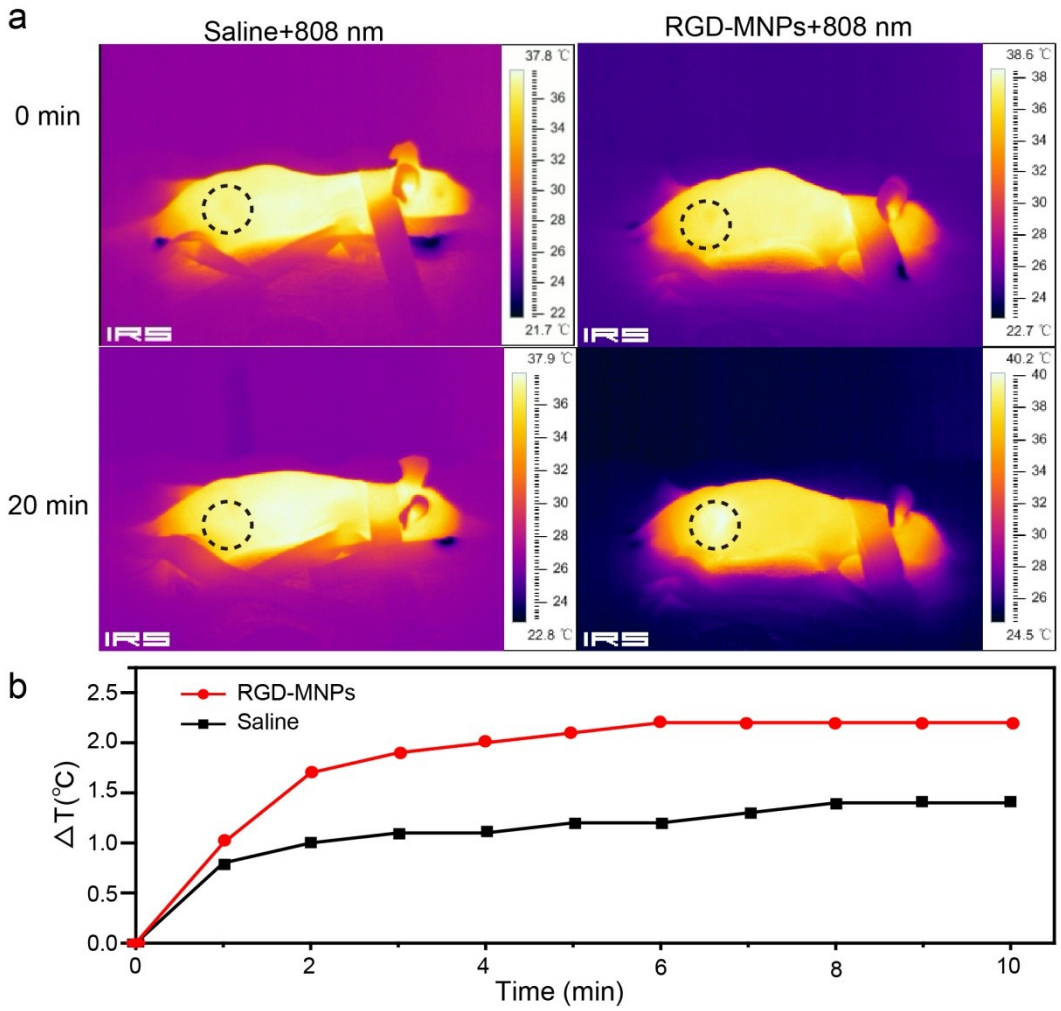

Figure S19. (a) IR thermal images of tumor-bearing mice exposed to the NIR laser (808 nm, 0.5 W cm^{-2}, 10 min) after i.v. injection with saline and RGD-MNPs (40 mg kg^{-1} of body weight), respectively. (b) Tumor temperatures of mice monitored by the IR thermal camera during laser irradiation as indicated in (a).

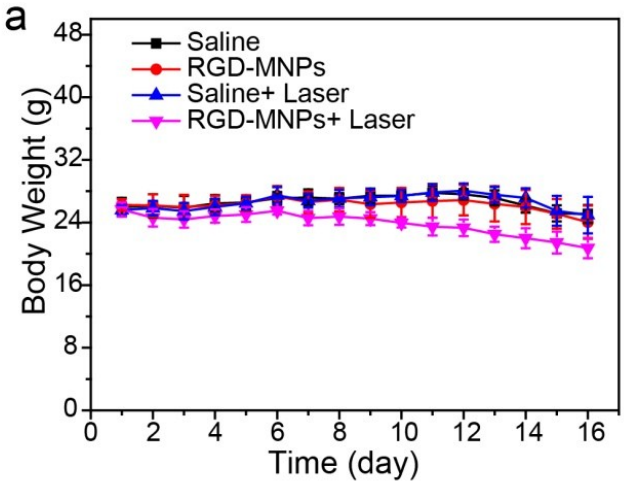

Figure S20. Body weights of mice after various treatments(4 mice per group).